liquid-phase nitrations. A logarithmic plot of the partial rate factors of monosubstituted benzenes, calculated from the data of Table III, vs. the σ^+ constants of the substituents is illustrated in Figure 2. With the exception of the two most activated substrates (vide infra) the data obey the least-squares fitted Hammett's type equation

$$\log f = \rho\sigma^+$$

characterized by a ρ value of −3.87, a negligible (<0.01) intercept, and a correlation coefficient of 0.96.

Considering that the σ^+ constants used for the plot are the classical ones, derived from condensed-phase studies, the success of their correlation with the present gas-phase data is remarkable. As a suitable comparison term, one can cite the nitration of nine aromatic substrates, carried out at 25 °C in nitromethane or acetic anhydride solutions, characterized by a ρ value of −6.53 with a correlation coefficient of 0.97,[6,33-36] and the nitration of 18 monosubstituted benzenes in sulfuric acid at 25 °C, characterized by a ρ value of −9.7.[37]

The less negative value of the ρ constant measured in the gas phase is suggestive of a more reactive and less selective electrophile than in liquid-phase nitrations, consistent with the free state of I, lacking both a solvation shell and a closely associated counterion, in that its charge is balanced by an electron far removed in the gas.

Another facet of the gas-phase reaction displays an intriguing analogy with liquid-phase nitrations. All highly activated substrates investigated, including mesitylene, *m*-xylene, and pentamethylbenzene, in addition to the aforementioned monosubstituted benzenes (PhOMe and c-Pr-Ph), are nitrated at significantly *lower* rates than expected from the correlation valid for less activated substrates. Such behavior is noteworthy, since it represents the gas-phase counterpart of the "encounter-rate" nitrations occurring in solution, where the two reactant molecules are held together for some time by a barrier to diffusion, related to the solvent viscosity. In the case of highly activated substrates, nitration occurs during the lifetime of such "encounter pairs" and its rate becomes diffusion-controlled, being limited by the encounter rate of the reactants.[6] It is conceivable that the "encounter-rate" nitration observed in the gas phase can involve a kinetically equivalent, if physically quite different, type of complex. In fact, ion–molecule reactions are believed to proceed in the gas phase via the preliminary formation of loose complexes, bound by strong electrostatic interactions between the unsolvated reactants.[38] When sufficiently activated aromatics are involved, nitration by I can be envisaged to occur during the lifetime of such complexes, kinetically equivalent to the "encounter pairs" postulated in solution, although the association of the reactants depends on electrostatic interactions, rather than on the solvent viscosity. Under such conditions, the rate of the gas-phase nitration would correspond to the capture rate of the ionic reactant by the neutral molecule (ADO or Langevin limit) and could not be increased by further enhancing the activation of the aromatic molecule, thus causing the observed loss of substrate selectivity.

Support for this interpretation is currently sought in our laboratory by temperature-dependence studies and by modulating the reactivity of the $RO^+(H)NO_2$ nitrating agent with appropriate modifications of the R group.

Conclusion

We have gone some way to extending the study of aromatic nitration to the gas phase, using an integrated approach which provides mechanistic information comparable to that available from solution-chemistry studies, allowing, in particular, the crucial evaluation of substrate and positional selectivity.

Resolving earlier discrepancies, the results point to the fundamental similarity of gas-phase and liquid-phase nitration, vindicating the expectation that mechanistic insight from one domain will be relevant to the other.

Acknowledgment. This work has financially been supported by the Italian National Research Council (C.N.R.) and the Ministry of Pubblica Istruzione. The authors thank G. de Petris, University of Rome "La Sapienza", for CID spectra, R. Gabrielli of the Servizio FTMS of the Area della Ricerca di Roma, C.N.R., for PA measurements, and O. Mõ for his contribution to theoretical calculations, carried out at the UAM/IBM Centers, Madrid.

Registry No. HPh, 71-43-2; MePh, 108-88-3; EtPh, 100-41-4; *n*-PrPh, 103-65-1; *i*-PrPh, 98-82-8; c-PrPh, 873-49-4; *t*-BuPh, 98-06-6; PhPh, 92-52-4; MeOPh, 100-66-3; FPh, 462-06-6; ClPh, 108-90-7; CF_3Ph, 98-08-8; C_6D_6, 1076-43-3; $MeONO_2{\cdot}H^+$, 99573-80-5; $MeONO_2$, 598-58-3; mesitylene, 108-67-8.

(33) Ingold, C. K.; Lapworth, A.; Rothstein, E.; Ward, D. *J. Chem. Soc.* **1931**, 1959.
(34) Ingold, C. K.; Smith, M. S. *J. Chem. Soc.* **1938**, 905.
(35) Bird, M. L.; Ingold, C. K. *J. Chem. Soc.* **1938**, 918.
(36) Roberts, J. D.; Sanford, J. K.; Sixma, F. L. J.; Cerfontain, H.; Zagt, R. *J. Am. Chem. Soc.* **1954**, *76*, 4525.
(37) Katritzky, A. R.; Clementi, S.; Tarhan, H. O. *J. Chem. Soc, Perkin Trans. 2*, **1975**, 1624.
(38) Magnera, T. F.; Kebarle, P. *Ionic Processes in the Gas Phase*; Almoster Ferreira, M. A., Ed.; Reidel Co.: Dordrecht, 1983; p 15 and references therein.

Wavelength-Dependent Photofragmentation of Gas-Phase $Mn_2(CO)_{10}$

D. A. Prinslow and V. Vaida*

Contribution from the Department of Chemistry and Biochemistry, University of Colorado, Boulder, Colorado 80309-0215. *Received January 2, 1987*

Abstract: $Mn_2(CO)_{10}$ is photolyzed at 350, 248, and 193 nm in the gas phase. Excitation of the σ^* state produces $Mn_2(CO)_8$ and $Mn(CO)_5$ fragments, indicating that this state is responsible for both metal–metal bond homolysis as well as ligand loss. Excitation of the π^* state at 248 and 193 nm leads to ligand loss with no evidence of metal–metal bond homolysis.

The formally single bond of dimanganese decacarbonyl was among the first metal–metal bonds to be characterized.[1] The simple structure of this molecule consisting of two $Mn(CO)_5$ subunits joined by a single metal–metal bond provides an ideal system for developing electronic structure theories.[2-4] The high quantum yield for dissociation of $Mn_2(CO)_{10}$, like that of most transition metal carbonyls, shortens the excited-state lifetimes and

(1) Dahl, L. F.; Ishishi, E.; Rundle, R. E. *J. Chem. Phys.* **1957**, *26*, 1750.
(2) (a) Levenson, R. A.; Gray, H. B. *J. Am. Chem. Soc.* **1975**, *97*, 6042. These are ionic bond dissociation energies and are used in the absence of available bond dissociation energies for the neutral molecule. (b) Levenson, R. A.; Gray, H. B.; Ceasar, G. P. *Ibid.* **1970**, *92*, 3653.

0002-7863/87/1509-5097$01.50/0

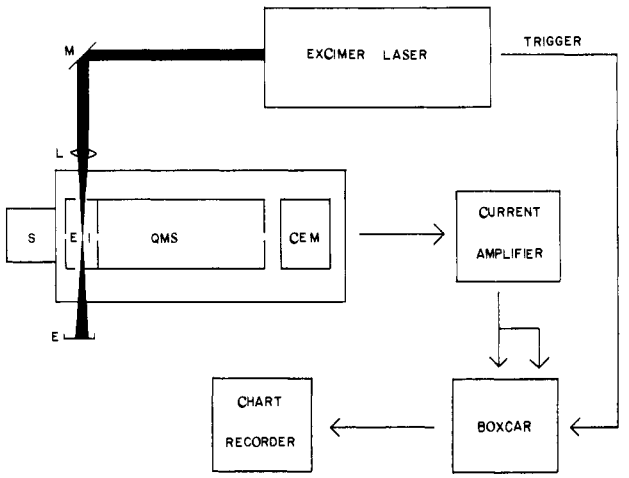

Figure 1. Block diagram of experimental apparatus. S = source, EI = electron impact ionizer and focusing elements, QMS = quadrupole mass filter, CEM = channeltron electron multiplier, M = mirror, L = lens, and E = energy meter.

consequently results in structureless electronic spectra and unmeasurably small quantum yields for emission. In the case of such highly dissociative organometallic compounds, the data used to test chemical theories of excited-state bonding and reactivity come from photochemical experiments.[3]

The condensed-phase photochemistry of $Mn_2(CO)_{10}$ has been reviewed recently.[5] In this molecule, both heterolytic cleavage of the Mn–CO bond and cleavage of the Mn–Mn bond are known to occur.[2b,3,5-20] The majority of earlier photochemical studies of $Mn_2(CO)_{10}$ explored the reactions of the lowest excited singlet state in the near-ultraviolet.[3] According to the molecular orbital description,[2] excitation into this strong $\sigma \rightarrow \sigma^*$ band should lead to a reduction of the metal–metal bond order to zero and therefore result in homolytic cleavage into $Mn(CO)_5$ units. Condensed-phase experiments did at first seem to agree with this prediction.[7,21-23] However, modern studies have found both metal–metal bond cleavage and CO loss to be important photochemical pathways.[9a,14,17,20,24] Time-resolved solution studies following UV photolysis of $Mn_2(CO)_{10}$ showed that both $Mn(CO)_5$ and $Mn_2(CO)_9$ are generated.[13-15,19] The structure of both of these radicals was studied using IR spectroscopy.[9,11,13] Hepp and Wrighton[9a] report that at 355 nm ≈30% of the photodissociated $Mn_2(CO)_{10}$ isolated in alkane matrices reacts by dissociative CO loss. The quantum yield for dissociation of $Mn_2(CO)_{10}$ in solution has been measured as a function of excitation energies:[15] the ratio of the quantum yield for formation of $Mn(CO)_5$ to that for $Mn_2(CO)_9$ varies from 0.74 at 355 nm to 0.21 at 266 nm. The interpretation of the condensed-phase results is complicated by the effects of sample interactions with the solvent or matrix, effects which are beyond the current capabilities of theoretical techniques. Photochemical experiments on transition metal complexes in the gas phase, under collision-free conditions, are being devised in order to provide a data base directly relevant to theory.[17,20]

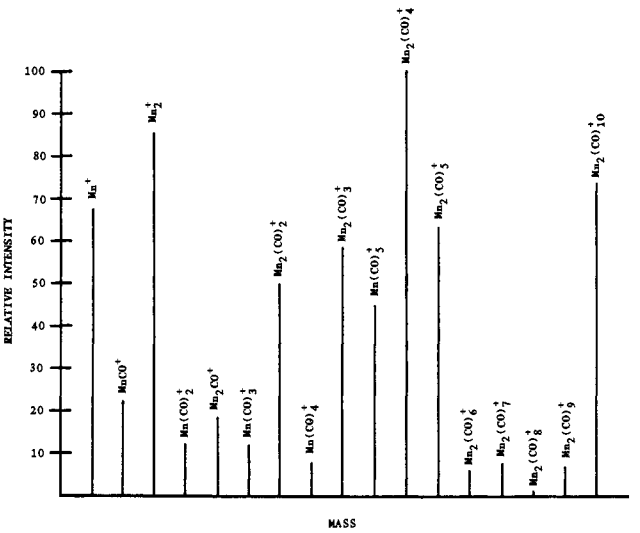

Figure 2. The 40-eV electron impact mass spectrum of $Mn_2(CO)_{10}$ with 7.5 mA of emission current.

In this paper, the gas-phase photodissociation of $Mn_2(CO)_{10}$ is studied using laser photolysis in conjunction with electron impact ionization/mass spectroscopic detection of the primary photofragments, allowing unambiguous identification of signal carriers. The wavelength-dependent photochemistry of this molecule is reported at 350, 248, and 193 nm.

Experimental Section

In this experiment, gas-phase $Mn_2(CO)_{10}$ is photodissociated and the fragments are detected by an electron impact ionization quadrupole mass spectrometer. With this apparatus we are able to observe primary photodissociation events by measuring the effect of the photolyzing laser on the electron impact ion current for each fragment of the parent molecule. A block diagram of the apparatus is shown in Figure 1.

Electron impact ionization (EI) is chosen over multiphoton ionization (MPI) for this experiment because of its ability to allow the observation of *all* fragment ions as seen in the EI mass spectrum of $Mn_2(CO)_{10}$ in Figure 2. Although the electron impact mass spectra of the possible photofragments are unknown, Figure 2 shows that all possible fragment ions are observable. MPI of metal carbonyls leads to the production and observation of primarily decarbonylated species.[25] This is because MPI involves resonances with one or more repulsive electronic surfaces of the primary fragment where dissociation competes favorably with ionization. EI, on the other hand, bypasses these dissociative excited states and leads to direct ionization of primary photofragments. The extent to which the ions are then fragmented by EI depends on the energy difference between the electron energy and the ionization potential of the fragment. The electron energies used in these studies were the lowest values with which a signal could be observed.

$Mn_2(CO)_{10}$, obtained from Strem Chemicals and used without further purification, is sublimed at 40 °C in a heated stainless steel cylinder located inside a vacuum chamber that is maintained at 10^{-6} torr by a liquid nitrogen trapped 6-in. diffusion pump. The sample effuses through a 1-mm orifice and into the ionization region of the mass spectrometer located 3 cm away.

(3) Geoffroy, G. L.; Wrighton, M. S. *Organometallic Photochemistry*; Academic Press: New York, 1979.
(4) Hoffmann, R. *Science* **1981**, *211*, 995.
(5) Meyer, T. J.; Casper, J. V. *Chem. Rev.* **1985**, *85*, 187.
(6) Coville, N. J.; Stolzenberg, A. M.; Muetterties, E. L. *J. Am. Chem. Soc.* **1983**, *105*, 2499.
(7) Hughey, J. L., IV; Anderson, C. P.; Meyer, T. J. *J. Organomet. Chem.* **1977**, *125*, C49.
(8) Fox, A.; Poe, A. *J. Am. Chem. Soc.* **1980**, *102*, 2497.
(9) (a) Hepp, A. F.; Wrighton, M. S. *J. Am. Chem. Soc.* **1983**, *105*, 5934. (b) Dunkin, I. R.; Hartner, P.; Shields, C. J. *Ibid.* **1984**, *106*, 7248.
(10) Bray, R. G.; Seidler, P. F., Jr.; Gethner, J. S.; Woodin, R. L. *J. Am. Chem. Soc.* **1986**, *108*, 1312.
(11) Church, S. P.; Poliakoff, M.; Timney, J. A.; Turner, J. J. *J. Am. Chem. Soc.* **1981**, *103*, 7515.
(12) Poliakoff, M. *Chem. Soc. Rev.* **1978**, *2*, 527.
(13) Church, S. P.; Hermann, H.; Grevels, F.; Schaffner, K. *J. Chem. Soc., Chem. Commun.* **1984**, 785 and references therein.
(14) Rothberg, L. J.; Cooper, N. J.; Peters, K. S.; Vaida, V. *J. Am. Chem. Soc.* **1982**, *104*, 3536.
(15) Yasufuku, K.; Kobayashi, T.; Iwai, J.; Yesaka, H.; Noda, H.; Ohtani, H. *Coord. Chem. Res.* **1985**, *64*, 1.
(16) Freedman, A.; Bersohn, R. *J. Am. Chem. Soc.* **1978**, *100*, 4116.
(17) Leopold, D. G.; Vaida, V. *J. Am. Chem. Soc.* **1984**, *106*, 3720.
(18) Burdett, J. K. *J. Chem. Soc., Faraday Trans. 2* **1974**, *70*, 1599.
(19) (a) Walker, H. W.; Herrick, R. S.; Olsen, R. J.; Brown, T. L. *Inorg. Chem.* **1984**, 23, 3748. (b) Herrick, R. S.; Brown, T. L. *Ibid.* **1984**, 4550.
(20) Seder, T. A.; Church, S. P.; Weitz, E. *J. Am. Chem. Soc.* **1986**, *108*, 7518.
(21) Wrighton, M. S.; Graff, J. L.; Luong, J. C.; Reichel, C. L.; Robbins, J. L. *Reactivity of Metal-Metal Bonds*; Chisholm, M. H., Ed.; American Chemical Society: Washington, DC, 1981.
(22) Wegman, R. W.; Olsen, R. J.; Gard, D. R.; Faulkner, L. R.; Brown, T. L. *J. Am. Chem. Soc.* **1981**, *103*, 6089.
(23) Waltz, W. L.; Hackelberg, O.; Dorfman, L. M.; Wojcicki, A. *J. Am. Chem. Soc.* **1978**, *100*, 7259.
(24) Yesaka, H.; Kobayashi, T.; Yasufuku, K.; Nagakura, S. *J. Am. Chem. Soc.* **1983**, *105*, 6249.
(25) Hollingsworth, W. E.; Vaida, V. *J. Phys. Chem.* **1986**, *90*, 1235.

Table I. Effect of Photolysis at 350 nm and 7.1×10^5 W/cm^2 on the Electron Impact Ion Current Intensity of Each Fragment of $Mn_2(CO)_{10}$

fragment ion	% change in EI		fragment ion	% change in EI	
Mn^+	0.0		$Mn(CO)_5^+$	+1.5	√
$MnCO^+$	0.0		$Mn_2(CO)_4^+$	+0.4	
Mn_2^+	+0.6		$Mn_2(CO)_5^+$	0.0	√
$Mn(CO)_2^+$	0.0		$Mn_2(CO)_6^+$	0.0	√
$Mn_2(CO)^+$	0.0		$Mn_2(CO)_7^+$	0.0	√
$Mn(CO)_3^+$	0.0	√[a]	$Mn_2(CO)_8^+$	+28.6	√
$Mn_2(CO)_2^+$	+0.6		$Mn_2(CO)_9^+$	0.0	√
$Mn(CO)_4^+$	0.0	√	$Mn_2(CO)_{10}^+$	0.0	√
$Mn_2(CO)_3^+$	0.0				

[a] A check indicates that this fragment could be produced by single photon excitation of $Mn_2(CO)_{10}$ at this wavelength (see Discussion).

Table II. Effect of Photolysis at 248 nm and 2.4×10^6 W/cm^2 on the Electron Impact Ion Current Intensity of Each Fragment of $Mn_2(CO)_{10}$

fragment ion	% change in EI		fragment ion	% change in EI	
Mn^+	+280.0		$Mn(CO)_5^+$	0.0	√
$MnCO^+$	0.0	√[a]	$Mn_2(CO)_4^+$	+0.5	
Mn_2^+	+47.5		$Mn_2(CO)_5^+$	+1.1	√
$Mn(CO)_2^+$	0.0	√	$Mn_2(CO)_6^+$	0.0	√
$Mn_2(CO)^+$	0.0		$Mn_2(CO)_7^+$	0.0	√
$Mn(CO)_3^+$	0.0	√	$Mn_2(CO)_8^+$	0.0	√
$Mn_2(CO)_2^+$	0.0		$Mn_2(CO)_9^+$	+2.5	√
$Mn(CO)_4^+$	0.0	√	$Mn_2(CO)_{10}^+$	0.0	√
$Mn_2(CO)_3^+$	+1.2				

[a] A check indicates that this fragment could be produced by single photon excitation of $Mn_2(CO)_{10}$ at this wavelength (see Discussion).

Electron impact ionization is performed using 40 eV of electron energy and 7.5 mA of emission current. Ideally, the electron energy should be chosen to be greater than the neutral fragment's ionization potential but less than its appearance potential from the parent molecule. Unfortunately, operation at these low electron energies (~10 eV) would restrict us to the use of emission currents that are too low to allow observation of fragments with our apparatus. Our choice of electron energy allowed us to observe a sufficient number of photofragments while keeping fragmentation due to EI to a minimum.

The excimer laser used in this experiment is a Lumonics TE-861T-4 operating at 90 Hz and at 350, 248, or 193 nm using fluxes from 1.0×10^4 to 2.4×10^6 W/cm^2. The particular laser flux used is selected to minimize multiphoton events while producing a sufficient number of primary (one photon) photofragments to be detected with an acceptable signal-to-noise ratio. The laser beam propagates perpendicular to the molecular beam axis and intersects it in the center of the ionization region of the mass spectrometer. The laser beam is slightly defocussed in order to minimize multiphoton effects. All positive ions are then directed into the quadrupole by a set of ion optics. The quadrupole used in this experiment, an Extranuclear Laboratories 4-270-9, has a resolution ($M/\Delta M$) greater than 1500 at mass 390 and a mass range of 2–500 m/q.

Ions transmitted by the quadrupole are amplified by a channeltron electron multiplier (CEM) and a current amplifier. The CEM has a gain of about 10^7, and the current amplifier has a variable gain of 10^4–10^6 V/A. The output voltage of the amplifier is split and sent to two gated integrators (EGG 164) of an EGG 162 Boxcar Integrator. The first gate measures the ion current intensity as produced by EI alone. The second gate measures the ion signal with the laser on (i.e., including the effects of photolysis). The difference between the two gates is obtained and averaged for ≈12 000 pulses. This difference, when divided by the electron impact ion current intensity, measured by the first gate, yields the percentage change in the electron impact ion current intensity for each fragment ion. It is this value that is tabulated for each fragment ion in Tables I and II.

The most significant source of noise in this experiment comes from fluctuations in the electron impact ion current. It is estimated that the data in Tables I and II are accurate to within ±20% of their respective values.

Results

Tables I and II show the percentage change in the electron impact ion current intensity for each fragment of $Mn_2(CO)_{10}$ as a result of photolysis at 350 and 248 nm, respectively.

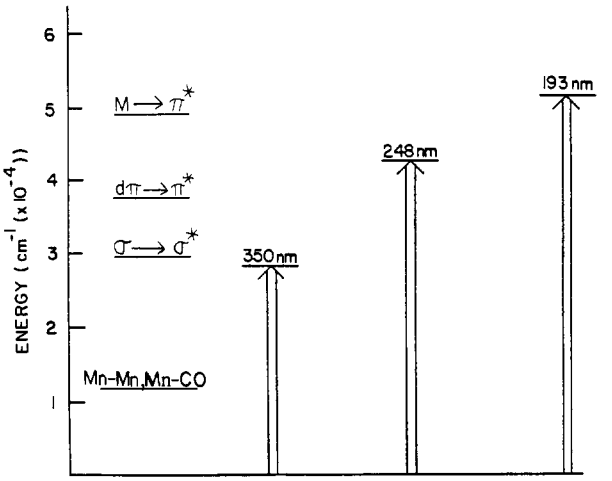

Figure 3. Absorption band maxima and their assignments (2) are shown along with the energies of the photolysis photons used in this experiment. For comparison, the Mn–Mn (27) and Mn–CO (28) bond strengths are displayed on the same energy scale.

Photolysis at 350 nm and 7.1×10^5 W/cm^2 (Table I) produces fragments which are indicative of two competing processes: metal–metal bond homolysis and metal–ligand bond breakage. The electron impact ion current intensities for $Mn_2(CO)_8^+$ and $Mn(CO)_5^+$ are seen to increase by 29 and 2%, respectively. The ion current intensities for smaller fragments are seen to increase as well; however, these fragments could not be produced via single photon excitation of $Mn_2(CO)_{10}$ and are the likely result of further fragmentation by EI. A control experiment was performed by monitoring the ions produced via MPI processes at this intensity by the laser alone. These MPI processes were found not to be important. However, at higher laser fluxes, fragment ions generated by the laser were observed indicating that MPI processes do begin to operate.

Photolysis at 248 nm and 2.4×10^6 W/cm^2 results in the appearance of fragments produced only by metal–ligand bond homolysis. Ion current intensities for $Mn_2(CO)_9^+$ and $Mn_2(CO)_5^+$ increase by 2 and 1%, respectively.[26] $Mn_2(CO)_9$ is undeniably a primary photoproduct at this wavelength. It has only one possible precursor ($Mn_2(CO)_{10}$) and its ion is not produced via MPI processes. No changes are observed in the ion current intensity for any of the $Mn(CO)_x^+$ (x = 1–5) fragments. As with 350-nm photolysis, increases in laser flux result in increased occurrence of multiphoton processes while decreases in flux lead to no observable signal.

Photolysis at 193 nm and 1.0×10^4 W/cm^2 was also briefly explored. At this wavelength and laser flux, $Mn_2(CO)_5^+$ was the predominant fragment whose ion current intensity was seen to increase upon photolysis.

Discussion

In the experiments reported here, photolysis of $Mn_2(CO)_{10}$ is performed in two electronic states of the molecule and the primary photofragments at each energy are identified. Figure 3 summarizes the energetic constraints of this experiment. The energies of the three transitions studied are displayed on the same scale with the laser photolysis energies and the Mn–Mn[27] and average Mn–CO[28] bond strengths.

The bond dissociation energies for this molecule are still the objects of extensive study.[27,29–31] The recent values for the Mn–Mn bond energy range from 25 to 41 kcal/mol, while the best value for the energy required for dissociation of the first

(26) A similar percentage increase in the ion current intensity of $Mn_2(CO)_8^+$ would be below the limits of our sensitivity.

(27) Goodman, J. L.; Peters, K. S.; Vaida, V. *Organometallics* **1986**, *5*, 815.
(28) Wawersik, H.; Basolo, F. *Inorg. Chim. Acta* **1969**, *3*, 113.
(29) Harel, Y.; Adamson, A. W. *J. Phys. Chem.* **1986**, *90*, 6693.
(30) Marcomini, A.; Poe, A. *J. Chem. Soc., Dalton Trans.* **1984**, 95.
(31) Martinho Simoes, J. A.; Schultz, J. C.; Beauchamp, J. L. *Organometallics* **1985**, *4*, 1238.

carbonyl is approximately 36 kcal/mol.[28] Using these numbers and average values for the dissociation energy of subsequent carbonyls,[32] we are able to estimate which fragments could be the result of one-photon excitation of the parent molecule, based on energetic considerations. These fragments are marked with a check in Tables I and II. We also estimate that at all photolysis energies used a large amount of excess energy is deposited in the primary fragments.

$Mn_2(CO)_{10}$ provides an ideal system in which to explore the competition between metal–metal and metal–CO bond reactivity in the excited electronic state. Excitation of the allowed $\sigma \rightarrow \sigma^*$ transition reduces the formal metal–metal bond order from 1 to 0. Accordingly, earlier condensed-phase photochemical data indicated clean, efficient homolytic cleavage to 17 electron $Mn(CO)_5$ radicals.[7,21-23] Modern condensed-phase studies[8,9a,14,24] have since established a more complex photochemical pathway for $Mn_2(CO)_{10}$ in this electronic state. It involves two primary photoproducts, due to Mn–Mn bond homolysis and to CO loss, whose relative yields are sensitive to environmental effects. Experiments designed to explore the photochemical properties of this molecule in gas phase, in the absence of solvent cage effects, are currently in progress.[17,20]

The results reported here establish directly the nature of photoproducts generated on excitation of $Mn_2(CO)_{10}$ into the σ^* state using 350-nm photons. Approximately equal amounts of $Mn_2(CO)_8^+$ and $Mn(CO)_5^+$ are generated on photolysis at this energy. These results are obtained at the lowest laser flux at which signal can be obtained in our instrument. The relative intensities and extent of fragmentation are extremely dependent on laser flux. At higher laser fluxes multiphoton processes become important and highly dissociated fragments, such as Mn^+, Mn_2^+, $Mn(CO)^+$, and $Mn_2(CO)_3^+$, dominate the spectrum. This extreme dependence on laser flux makes this system difficult to study by less direct techniques.

The results presented establishing the existence of two gas-phase photochemical pathways, metal bond homolysis and CO loss, agree well with results obtained spectroscopically using time-resolved IR absorption and MPI techniques.[17,20] The photochemistry of the S_1 state of $Mn_2(CO)_{10}$ in the gas phase is found to be consistent with that of the molecule in solution.[14,24]

The energy dependence of the photochemistry of this molecule is investigated by excitation of the π^* state. At 248 nm ($d\pi \rightarrow \pi^*$ transition) the primary photofragment detected is $Mn_2(CO)_9$, with no detectable metal bond homolysis products. The trend continues as excitation at 193 nm ($M \rightarrow \pi^*$ transition) yields only $Mn_2(CO)_5$. This fragment is presumably formed by CO loss from the initially formed, highly excited $Mn_2(CO)_9$.

The energy dependence of the photochemistry of $Mn_2(CO)_{10}$ is consistent both with the conclusions of time-resolved gas-phase studies and time-resolved experiments in solution.[14,20,24]

Conclusion

The photochemistry of $Mn_2(CO)_{10}$ in the gas phase is investigated with a direct experiment based on mass spectroscopic detection of primary photofragments. The results indicate that excitation of the σ^* state leads to both metal bond homolysis and ligand loss. Excitation of the π^* state leads to ligand loss. These results agree with recent studies of the photochemistry of this molecule both in gas and condensed phases. The extensive information now available establishes $Mn_2(CO)_{10}$ as the first transition metal cluster complex for which a comprehensive picture of the chemistry of the electronic states is available.

Acknowledgment. Financial support from the National Science Foundation (Grant No. CHE-8607697) is gratefully acknowledged. We wish to thank Professor E. Weitz for making their data on $Mn_2(CO)_{10}$ available to us prior to its publication.

(32) Svec, H. J.; Junk, G. A. *J. Am. Chem. Soc.* **1967**, *89*, 2836.

The Structure of the Methylnitrene Radical

P. G. Carrick,[1a] C. R. Brazier,[1b] P. F. Bernath,*[1b] and P. C. Engelking*[1c]

Contribution from the Department of Physics, Mississippi State University, Mississippi State, Mississippi 39762, Department of Chemistry, University of Arizona, Tucson, Arizona 85721, and Department of Chemistry, University of Oregon, Eugene, Oregon 97403.
Received February 6, 1987

Abstract: The geometry and electronic spin–spin splitting have been determined for the methylnitrene radical by high-resolution gas-phase emission spectroscopy of the $\tilde{A}^3E$–$\tilde{X}^3A_2$ transition. The equivalent of the ESR D constant is 1.720 ± 0.004 cm^{-1}, significantly larger than the previously attributed value. The ground state C–N single bond (1.411 ± 0.001 Å) is noticeably shorter than that found in calculations on this radical or in other compounds containing a C–N single bond.

Methylnitrene (CH_3N, methylimidogen) introduces the series of alkylnitrene radicals. Small enough to allow good theoretical and experimental treatments, it provides numerous tests of our current understanding of the structure of nitrene radicals. Here we present the structure of methylnitrene as revealed by high resolution UV spectroscopy.

Two factors may complicate the electronic structure of the open-shell nitrene radical. First, the vacancies in the valence shell, formally localized in nonbonding p-orbitals on the nitrogen, may "delocalize", spreading toward the alkyl end of the radical. This would modify directly the H–C bonding and may add double bond character to the C–N bond. Second, the open-shell nitrogen may take advantage of having to attend to only one bond and adjust its own electronic structure to optimize this C–N bond. This would show up in an anomalous C–N single bond and possibly may modify the H–C bonding by changing the electronic structure at the carbon.

Calculations[2-4] indicate that the ground state of the nitrene radical is a triplet electronic state, $^3A_2$. Two electronic singlets

(1) (a) Mississippi State University. (b) University of Arizona. (c) University of Oregon.

(2) (a) Yarkony, D. R.; Schaefer, H. F., III; Rothberg, S.; *J. Am. Chem. Soc.* **1974**, *96*, 5974. (b) Demuynck, J.; Fox, D. J.; Yamaguchi, Y.; Schaefer, H. F., III. *J. Am. Chem. Soc.* **1980**, *102*, 6204.

(3) (a) Lathan, W. A.; Curtiss, L. A.; Hehre, W. J.; Lisle, J. B.; Pople, J. A. *Prog. Phys. Org. Chem.* **1974**, *11*, 175. (b) Pople, J. A.; Raghavachar, K.; Frisch, M. J.; Binkley, J. S.; Schleyer, P. v. *J. Am. Chem. Soc.* **1983**, *105*, 6389.

(4) Ha, T. K.; Nguyen, M. T. *THEOCHEM.* **1982**, *4*, 355.

0002-7863/87/1509-5100$01.50/0